GSA Data Repository 2015357

Eocene Atmospheric CO_2 from the Nahcolite Proxy

E. Jagniecki[1,2], T. K. Lowenstein[1], D. M. Jenkins[1], and R. V. Demicco[1]

[1]*Department of Geological Sciences and Environmental Studies, Binghamton University, Binghamton, New York 13902, USA.*

[2]*Current address: ConocoPhillips Company, 600 North Dairy Ashford, Houston, Texas 77079, USA.*

Data Repository:

Supporting text

List of terrestrial and marine proxies compiled in Figure 1:

Paleosols

Cerling, 1992; Koch et al., 1992; Quade et al., 1994; Sinha and Stott, 1994; Quade and Cerling, 1995; Ekart et al., 1999; Royer et al., 2001; Nordt et al., 2002; Retallack, 2009b; Cotton and Sheldon, 2012; Huang et al., 2013; Hyland and Sheldon, 2013; Hyland et al., 2013.

Stomatal Indices/Ratios

Van der Burgh et al., 1993; Kürshner, 1996; McElwain, 1998; Royer et al., 2001; Beerling et al., 2002; Greenwood et al., 2003; Royer et al., 2003; Kürshner et al., 2008; Retallack et al., 2009a; Smith et al., 2010; Doria et al., 2011; Grein et al., 2011; Stults et al., 2011; Erdei et al., 2012; Roth-Nebelsick et al., 2012; Grein et al., 2013; Franks et al., 2014.

Phytoplankton (Alkenones)

Seki et al., 2010; Badger et al., 2013a; Badger et al., 2013b; Zhang et al., 2013.

Marine Boron ($\delta^{11}B$)

Pearson et al., 2009; Seki et al., 2010; Bartoli et al., 2011; Foster et al., 2012; Badger et al., 2013a.

Liverwort

Fletcher et al., 2008.

Trona deposits discussed and illustrated in Figure 1 are:
(1) Beypazari, Turkey, Miocene (21.5 Ma ± 0.9 Ma) (Helvaci, 1998), and
(2) Searles Lake, California, USA, Pleistocene (< 1 Ma) (Smith, 1979).

All dates calibrated to the geologic timescale of Gradstein et al. (2004) (Royer, 2014).

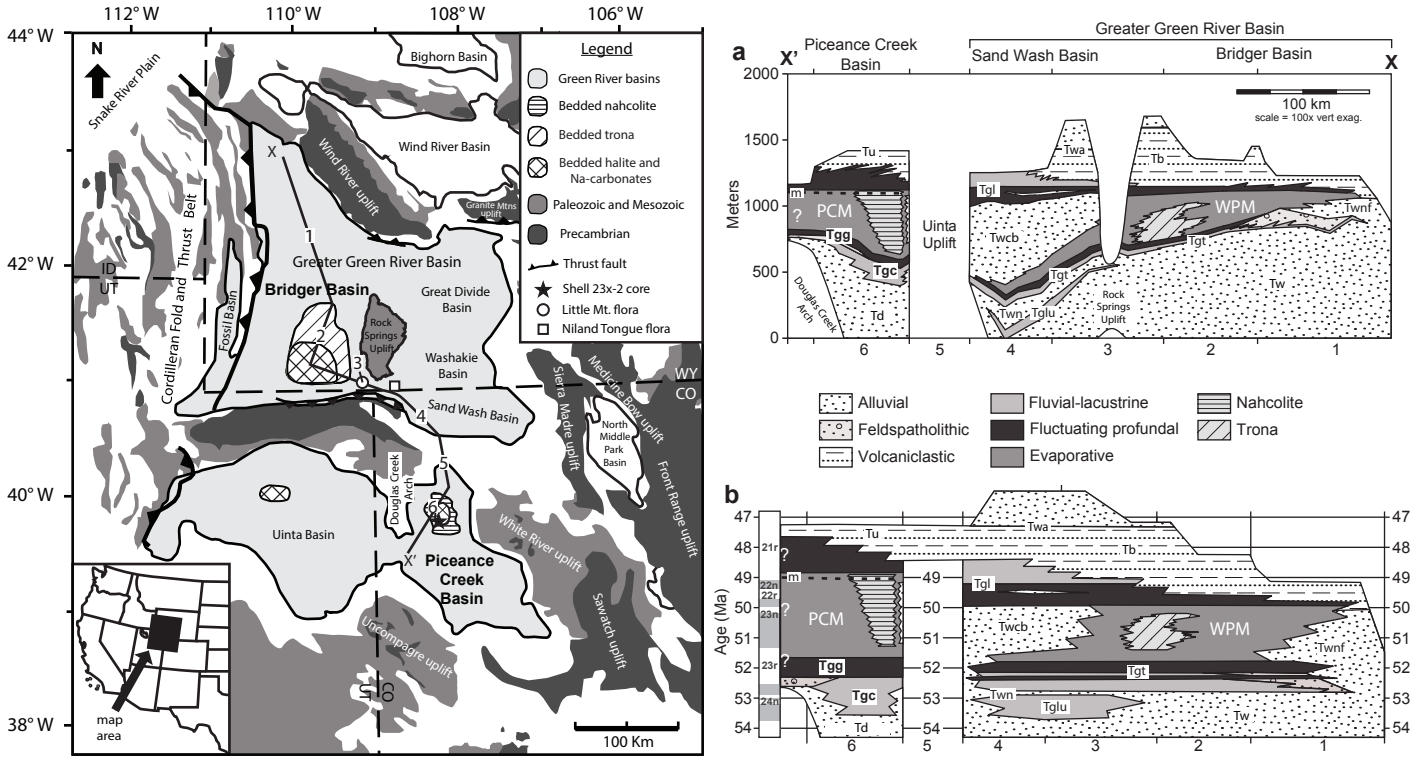

Figure DR1. General geologic map of Eocene Green River basins (Colorado and Wyoming, USA) and extent of saline deposits. Nahcolite occurs in the Piceance Creek Basin and trona in the Bridger Basin. Location of fossil leaf assemblages (circle and square) are from Wilf (2000). Lithostratigraphic (A) and time stratigraphic (B) cross sections show position and timing of Green River evaporite sedimentation. PCM—Parachute Creek Member; WPM—Wilkins Peak Member (see below for all other abbreviations). Modified from Smith and Carroll (2015) and Dyni (1996).

Abbrevations

Greater Green River Basin: WPM = Wilkins Peak Member, Tgl = Laney Member, Tgt = Tipton Member, Twa = Washakie Formation, Tb = Bridger Formation, Twcb = Cathedral Bluffs Tongue, Twnf = New Fork Tongue, Twn = Niland Tongue, Tglu = Lumen Tongue, Tw = Wasatch Formation; Piceance Creek Basin: Tu = Uinta Formation, m = Mahogany Zone, Tgg = Garden Gulch member, Tgc = Cow Ridge Member , Td = Debeque Formation.

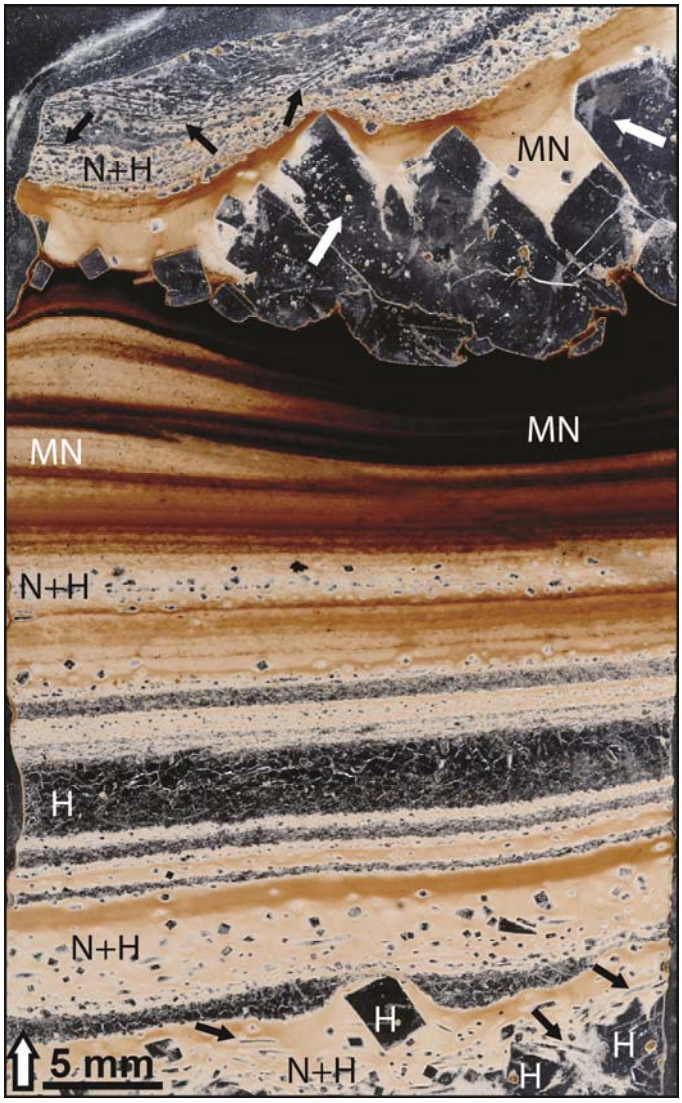

Figure DR2. Thin-section photomicrograph of primary nahcolite and halite, Piceance Creek Basin, Colorado (USA), with textures diagnostic of precipitation in perennial, density-stratified, saline lake. Microcrystalline nahcolite (MN) occurs as light brown to black organic-rich laminae; halite (H) occurs as clear crystalline layers in middle and larger individual cubes at bottom and top. Nahcolite + halite laminae (N + H) contain halite cubes and platy "rafts" (black arrows) indicating that crystals originally precipitated at air-water interface and sank to lake bottom to form layered accumulations. Fine nahcolite + halite crystal mud drapes vertical, widening-upward halite crystals that formed at brine bottom (top, white arrows). Arrow next to scale bar indicates up direction. Shell 23x-2 core, depth 561 m (39°54′19.67″N, 108°21′44.06″W, referenced to WGS84 datum) (see Fig. DR1 for location).

General Experimental Methods

All experiments were done using reagent-grade $NaHCO_3$ (nahcolite), Na_2CO_3, and $Na_2CO_3 \cdot 10H_2O$ (natron) and synthetic trona made from these chemicals. Experimental treatments used perfluoroalkoxy (PFA) capsules because of their unique property of being more permeable to CO_2 gas than water. All experiments were done with known concentrations of CO_2 gas (ppm) (±2%), verified with a LI-820 CO_2 gas analyzer (±0.4 ppm) (Li-Cor, Inc.), at temperatures of 10–75 °C, and near atmospheric pressure (<2 psi). Potential dissolution of fluorine from PFA tubing was tested by ion chromatographic analysis (Dionex ICS-2000) of water in contact with PFA tubing at 70 °C for 11 days; the results revealed negligible concentrations of fluoride (<1 ppm). Samples were analyzed by powder X-ray diffraction (XRD) using a Philips PW3040-MPD diffractometer operated at 40 kV and 20 nA using copper Kα X-rays. Reaction directions were determined by comparing changes in relative peak areas modeling the peak profiles using a symmetric pseudo-Voigt function (50% Gaussian). Trona was produced by mixing 1 mol of Na_2CO_3, 1 mol $NaHCO_3$, and 16.0 wt% H_2O to give a bulk composition of $Na_2CO_3 \cdot NaHCO_3 \cdot 2H_2O$. This mixture was then sealed in perfluoroalkoxy (PFA) capsules and reacted at 55 °C and 1 atm for 20 days to yield pure trona, as confirmed by powder XRD.

Nahcolite-trona experiments, reaction (1)

$$\mathbf{3NaHCO_{3\ (nahcolite)} + H_2O_{(l)} = Na_2CO_3 \cdot NaHCO_3 \cdot 2H_2O_{\ (trona)} + CO_{2\ (gas)}}$$

Reaction (1) experiments were conducted by first mixing and grinding stoichiometric proportions of nahcolite and trona in acetone. Approximately 6-10 mg of that mixture was packed in PFA capsules sealed at one end of a section of PFA tubing

(0.188 inch OD, 0.031 inch wall thickness) with a propane torch. Measured amounts of H_2O (typically 2.1 – 3.3 wt%) were added to each dry mixture. The PFA capsules were then crimped shut, clamped in a vice, flame sealed, and weighed to verify that no loss of water occurred during sealing. The measured amount of H_2O added to each dry mixture was corrected for small evaporation losses (0.0064 mg H_2O/5 minutes) prior to and during the sealing of PFA capsules. The PFA capsules were then placed in a stainless steel autoclave (1.0 inch OD, 0.625 inch ID, 3.5 inch length) that contained ~ 1ml of H_2O and equipped with a gas flow inlet and outlet. The ~ 1ml of H_2O ensured that water-vapor saturated conditions existed outside the PFA capsules and also prevented loss of water from inside capsules during experimental runs at elevated temperatures. A known concentration of CO_2 gas was initially flowed through the autoclave to purge the reaction chamber and then the gas inside the chamber was sealed off at $\leq$ 2 psi pressure. Autoclaves were then placed in a temperature-regulated water bath for experimental durations of 17 to 35 hours. Pressures inside the autoclaves were those of the vapor pressure of water and CO_2 gas at the temperature of interest. At the end of the experiments, the capsules were retrieved, dried, and weighed to verify no net loss or gain of mass that may have occurred from an improper seal. All samples were mounted for XRD analysis as a thin smear with acetone on a zero-background quartz plate and scanned over the range of 38-42 °2Θ. Peak area ratios (nahcolite/trona) from reaction products were compared to peak area ratios of starting reaction mixtures to determine the extent of forward or reverse reactions (Table DR1). An example of determining forward and reverse reaction directions at a constant CO_2 concentration of 1469 ppm (mole fraction) is illustrated in Figure DR3.

Nahcolite-Natron Experiments, Reaction (2)

$2NaHCO_{3\ (nahcolite)} + 9H_2O_{(l)} = Na_2CO_3 \bullet 10H_2O_{\ (natron)} + CO_{2\ (gas)}$

A different approach for investigating reactions (2) and (3) had to be undertaken due to the large volume of H_2O needed for each reaction and the sensitivity of natron to dehydration at room temperature. For these reasons, all reaction mixtures were prepared at room temperature in a humidified (water vapor saturated) chamber. It was also observed that nahcolite readily reacted and degassed CO_2 when a large quantity of water was added to a dry nahcolite-natron reaction mixture, making inconsistent background X-ray diffraction scans for the reaction (2) mixture. To overcome this problem it was necessary to investigate reaction (2) by in-situ X-ray diffraction in a sealed heating chamber (Anton Paar, HTK-10) equipped with a gas inlet and outlet. A damp sponge was placed inside the chamber to maintain vapor saturated conditions. Stoichiometric proportions of 2 moles of $NaHCO_3$ (nahcolite) and 1 mole $Na_2CO_3 \bullet\ NaHCO_3 \bullet 2H_2O$ (trona) were mixed and ground in liquid nitrogen. About 300 mg of that mixture was mounted on an aluminum sample holder (20 x 15 x 1.5 mm) with a glass slide backing plate and placed in the water vapor saturated chamber at room temperature. The correct stoichiometric proportion (9 moles of H_2O = 26.3 weight %) was added to the sample on the aluminum-glass holder and quickly placed into the heating chamber. The starting reaction mixture was analyzed by X-ray diffraction over the range of 41-46 °2Θ to determine initial nahcolite/natron peak area ratios in the presence of 9 moles of H_2O. At lower scanning angles (< 40 °2Θ) natron produced inconsistent peak heights due to its preferred orientation in water and peak overlap with trona. The heating chamber is normally used at temperatures > 25° C; however, lower temperatures, down to 10° C,

could be achieved by circulating cold water through the chamber housing. The heating chamber was purged with known concentrations of CO_2 that was first bubbled in distilled water to form water vapor-saturated CO_2 in the reaction chamber. The partial pressure of H_2O at these conditions has a minimal effect on lowering the concentration of CO_2. If there is such an effect the error is constrained between the experimental data determined by reaction (2) and within error of the known concentrations of CO_2 gas used. The chamber was then sealed at the gas inlet and outlet at a pressure of $\leq$ 2 psi. Reaction mixtures were held at constant temperature and CO_2 gas concentrations for 0.75 to 1 hour and then analyzed by X-ray diffraction to determine the extent of forward and reverse reactions by comparing the product peak area ratios to the starting reaction mixture peak area ratios. Two approaches were used to verify the extent of forward and reverse reactions at given experimental conditions: (1) maintain a constant CO_2 gas concentration and raise the temperature of the heating stage (10° to 21.5° C) and 2) maintain a constant temperature and vary CO_2 gas concentrations. Both approaches produced the same results (Table DR2).

Trona Natron Experiments, Reaction (3)

$$\mathbf{2Na_2CO_3 \bullet NaHCO_3 \bullet 2H_2O_{(trona)} + 25H_2O_{(l)} = 3Na_2CO_3 \bullet 10H_2O_{(natron)} + CO_{2\,(gas)}}$$

Reaction (3) experiments were prepared similarly to reaction (2) experiments, described above, but they did not require *in-situ* X-ray diffraction measurements because of the greater stability of trona and natron at room temperature. A mixture of 2 moles of trona and 3 moles of natron was prepared by grinding in a water vapor saturated chamber. That mixture was placed on an aluminum holder mounted on a glass slide. Following addition of 25 moles of H_2O (25 wt%), the reaction mixture was analyzed by X-ray

diffraction over a range of 31-36 °2Θ to determine the initial trona/natron peak area ratios. The sample holder with the reaction mixture was then placed on top of a stainless steel cylinder partially submerged in water inside a glass jar; the glass jar was equipped with gas inlet and outlet valves. The glass jar, with sample, and water added to maintain water-vapor saturated conditions, was then purged with a known concentration of CO_2 gas, sealed at ≤ 2 psi, and placed in a water bath at constant temperature (± 0.1° C) for 24 hours, time sufficient to reach equilibrium. The stainless steel cylinder ensured that the sample mixture maintained the temperature of the water bath. At the end of each experiment, the reaction products were immediately analyzed by X-ray diffraction to determine peak area ratios (trona/natron). Peak area ratios were then compared against the peak area ratios of starting reaction mixtures to identify the extent of forward or reverse reactions (Table DR3).

Thermodynamic calculations: Derivation of $\Delta H^{\circ}_{f,298}$, and S°_{298} for trona and natron

One goal of this study was to derive thermochemical data for trona and natron, and from that data, calculate the equilibrium boundaries for reactions (1), (2) and (3) in temperature-pCO_2 space (i.e., Fig. 3). Thermodynamic data are well known for nahcolite, CO_2, and H_2O, but trona and natron are not well constrained. Accurate values for the standard enthalpy of formation ($\Delta H^{\circ}_{f,298}$) and standard third-law entropy (S°_{298}) of trona and natron can be derived from our experimental data. In light of the limited temperature range (< 60° C) and constant total pressure of 1 atm, where enthalpy and entropy changes are essentially constant, the following expression was used:

$$\Delta G = 0 = \Delta H^{\circ}_{r,298} - T\Delta S^{\circ}_{r,298} + RT \ln K \quad (4)$$

where $\Delta G, \Delta H,$ and ΔS are changes in the Gibbs free energy, enthalpy, and entropy, respectively, and K is the equilibrium constant. To derive (ΔH_r°) and (ΔS_r°) of a given reaction, Eq. (4) can be simplified and rearranged to give:

$$-\Delta H_{r,298}^\circ + T\Delta S_{r,298}^\circ = RT \ln K \quad (5)$$

By setting $RT \ln K = G'$, Eq. (5) can be expressed as:

$$G' = T\Delta S_{r,298}^\circ - \Delta H_{r,298}^\circ \quad (6)$$

Equation (6) yields a straight line when plotting $G' vs. T$, in which the slope is $\Delta S_{r,298}^\circ$ and the y-intercept is $-\Delta H_{r,298}^\circ$ for a given reaction. Thermochemical data for nahcolite, CO_2, and H_2O were taken from Vanderzee (1982) and Robie and Hemingway (1995). Adopting a standard state of unit activity for the pure phases at the temperature of interest and noting that nahcolite, trona, and natron are pure phases, the equilibrium constant for reactions (1), (2), and (3) is simply:

$$K = \frac{[fCO_2]^{nCO2}}{[a_{H2O}]^{nH2O}} \quad (7)$$

where the value of the equilibrium constant is determined by the fugacity of CO_2 (f_{CO2}) and activity of H_2O (a_{H2O}) raised to their molar coefficients. Fugacity of CO_2 is the known concentration of CO_2 gas used in the experiments (expressed as mole fractions). The activity of H_2O, $a_w = 0.90,$ for reactions (1), (2), and (3), is fixed at the invariant point and was calculated by Hatch (1972) and Vanderzee (1982).

Figure DR4 shows plots of $G' vs.$ temperature for all three reactions. We obtained values of $\Delta S_{r,298}^\circ$ = 0.1246 ± 0.016 kJ/K and $\Delta H_{r,298}^\circ$ = -53.450 ± 4.89 kJ for reaction (1) using a linear regression of the data. It should be noted that the straight line in Fig. DR4(A) falls between all nahcolite-producing experiments (open circles) and trona-producing experiments (solid circles) illustrating internal consistency of the experimental data. With

these values the $\Delta H^{\circ}_{f,298}$ and S°_{298} for end-member trona can be derived from reaction (1) with the equations:

$$\Delta H^{\circ}_{f,298,trona} =$$

$$\Delta H^{\circ}_{r,298} - \Delta H^{\circ}_{f,298,CO2} + 3\left(\Delta H^{\circ}_{f,298,nach}\right) + \Delta H^{\circ}_{f,298,H2O}, \text{ and} \quad (8)$$

$$S^{\circ}_{298,trona} =$$

$$\Delta S^{\circ}_{r,298} - \Delta S^{\circ}_{298,CO2} + 3\left(\Delta S^{\circ}_{298,nach}\right) + \Delta S^{\circ}_{298,H2O} \quad (9)$$

where thermodynamic data exist for nahcolite, $CO_{2(g)}$, and $H_2O_{(l)}$, and values for $\Delta H^{\circ}_{r,298}$ and $\Delta S^{\circ}_{r,298}$ were derived above. Calculated $\Delta H^{\circ}_{f,298}$ and S°_{298} for trona are -2658.40 ± 0.55 kJ and 0.2868 ± 0.003 kJ/K, respectively. Uncertainties are constrained by our experimental data brackets (Fig. DR4, A). Similarly, $\Delta H^{\circ}_{f,298}$ and S°_{298} for natron can be derived from $G'\ vs.$ temperature for reaction (2), where a linear regression to all data yields $\Delta S^{\circ}_{r,298}$ = 0.1216 ± 0.026 kJ/K and $\Delta H^{\circ}_{r,298}$ = 20.585 ± 7.472 kJ (Fig. DR4, B) as:

$$\Delta H^{\circ}_{f,298,natron} =$$

$$\Delta H^{\circ}_{r,298} - \Delta H^{\circ}_{f,298,CO2} + 2\left(\Delta H^{\circ}_{f,298,nach}\right) + 9(\Delta H^{\circ}_{f,298,H2O}) \quad (10)$$

$$S^{\circ}_{298,natron} =$$

$$\Delta S^{\circ}_{r,298} - \Delta S^{\circ}_{298,CO2} + 2\left(\Delta S^{\circ}_{298,nach}\right) + 9(\Delta S^{\circ}_{298,H2O}) \quad (11)$$

The calculated $\Delta H^{\circ}_{f,298}$ and S°_{298} for natron are -4094.49 ± 0.60 kJ and 0.4993 ± 0.002 kJ/K, respectively, and their uncertainties were constrained by our experimental data. Due to the near vertical slope of the bracketed data for reaction (3) a suitable linear regression could not be obtained; however, the $\Delta H^{\circ}_{f,298}$ and S°_{298} values for trona and natron derived from reactions (1) and (2) could be combined to produce a straight-line relationship in $G'vs.T$ space that is consistent with the experimental data. In Figure DR4

(C) the dotted line is the linear regression to all of the experimental data; it misses the data point at 290 K (data point Tr-nat-m3-2). The solid line is the predicted $G'vs.T$, which conforms to all the experimental data because it lies to the right of solid circles and to the left of the open circles. The thermochemical data derived here are in close agreement with values derived by Vanderzee (1982) and are tabulated in Table DR4. Our derived enthalpy and entropy values for natron and trona are slightly different in part because the values of Vanderzee (1982) were calculated using earlier experimental pCO_2 and temperature data (Eugster, 1966) at standard state.

Using the thermochemical data derived here, the equilibrium phase boundaries (in pCO_2-temperature space) can be calculated by rearranging equation (4) and solving for the pCO_2 at any temperature. First, K can be expanded and equation (5) can be rewritten as:

$$-\Delta H^{\circ}_{r,298} - T\Delta S^{\circ}_{r,298} = \ RTln(pCO_2)^{n_{CO2}} - RTln(a_w)^{n_{H2O}} \quad (12)$$

and equation (12) can be rearranged to solve for pCO_2:

$$pCO_2 = \left[e^{\left(\frac{-\Delta H^{\circ}_{r,298} - T\Delta S^{\circ}_{r,298} + RTln(a_W)^{n_{H2O}}}{RT} \right)} \right]^{1/n_{CO2}} \quad (13)$$

The calculated boundaries are shown in Fig. 3 and DR4.

Equilibrium reaction boundaries and the activity of H_2O

Using our derived enthalpy and entropy values for natron and trona, changes in the activity of H_2O can be evaluated in the Na_2CO_3-$NaHCO_3$-CO_2-H_2O-NaCl system. By changing the activity of H_2O at variable brine concentrations, the shift in the equilibrium

phase boundaries and the invariant point can be observed. Figure DR5 shows the downward shift of all three phase boundaries with the lowering of the activity of H_2O. The invariant point shifts to lower pCO_2 and temperatures at halite saturation ($a_w = 0.75$). The effect of NaCl added to the Na_2CO_3-$NaHCO_3$-CO_2-H_2O system helps explain the formation of nahcolite at relatively low temperatures, such as was reported during the winter months and cold nights in Owens Lake, California, USA from 1970-1971 (Smith et al., 1987).

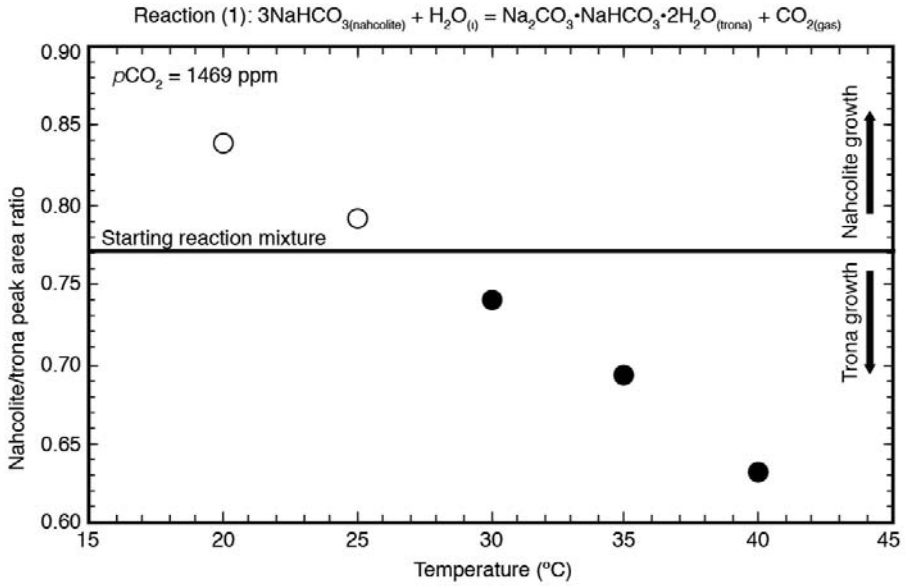

Figure DR3. Example of the method used in this study for determining sodium carbonate mineral stabilities as a function of temperature and pCO_2 from measured XRD peak-area ratios. Forward and reverse reactions were established for reaction (1) $3NaHCO_{3\ (nahcolite)} + H_2O_{(l)} = Na_2CO_3 \bullet NaHCO_3 \bullet 2H_2O_{\ (trona)} + CO_{2\ (gas)}$. Starting reaction mixture has nahcolite/trona ratio of 0.771 (horizontal line). Equilibrium temperature for the reaction at a CO_2 concentration of 1469 ppm is ~ 27° C in the system Na_2CO_3-$NaHCO_3$-H_2O-CO_2 (Table S1). Note that nahcolite/trona XRD peak-area ratios below the starting ratio of 0.771 indicate growth of trona relative to nahcolite at higher temperatures (black circles), whereas ratios above 0.771 indicate growth of nahcolite at lower temperatures (white circles). Uncertainty in temperature and peak-area ratios is the size of the symbol.

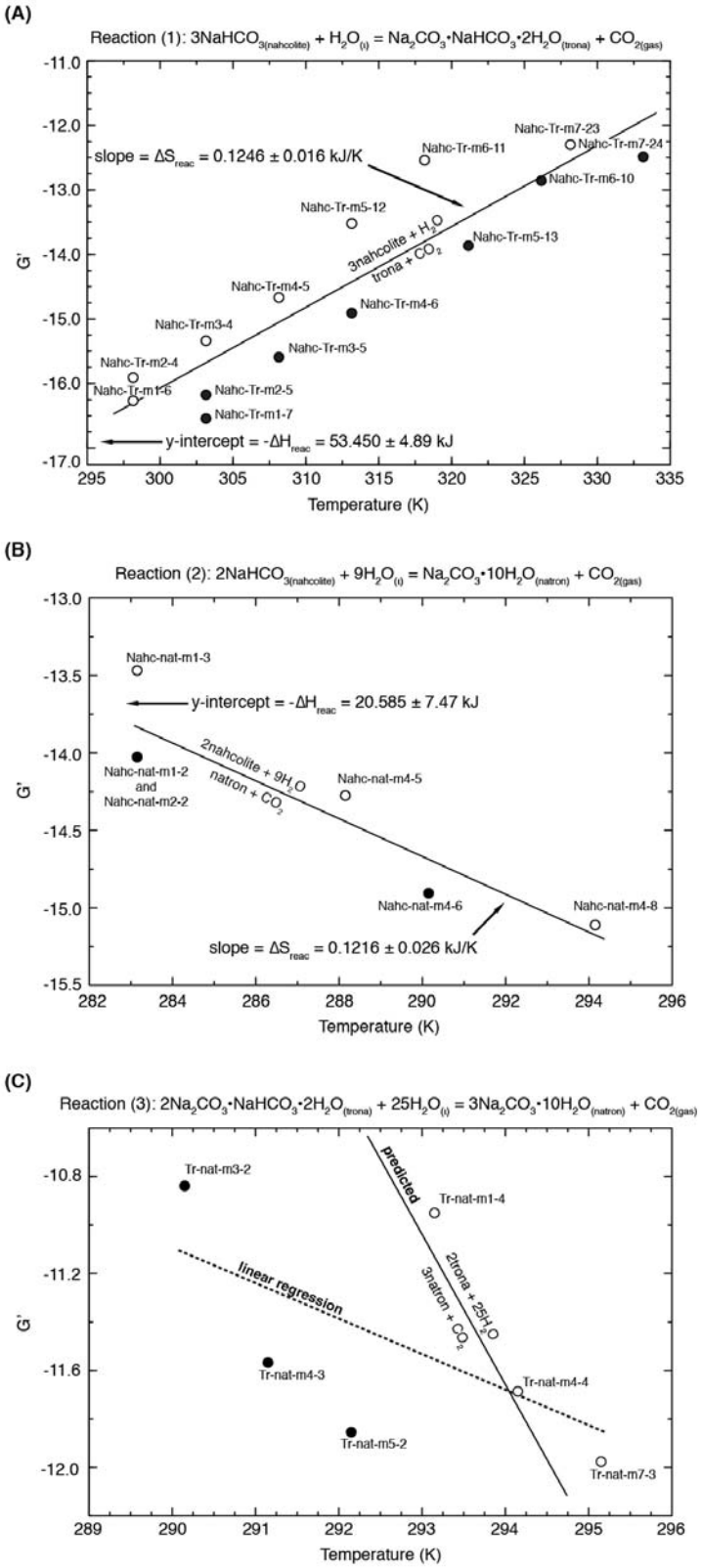

Figure DR4. G' *vs.* temperature plots for bracketed experimental data using *K* values derived from known concentrations of CO_2 gas used in the experiments and activity of

H_2O = 0.90, calculated after refs S33 and S34. G' = $RT \ln K$, where $K = \frac{[fCO_2]^{nCO2}}{[a_{H2O}]^{nH2O}}$. A). G' *vs.* temperature for reaction (1); solid black circles show reversal experiments where trona growth occurred and open circles indicate where nahcolite growth occurred. B) G' *vs.* temperature for reaction (2); solid circles show reversal experiments where natron growth occurred and open circles indicate nahcolite growth. Uncertainties for the data in (A) and (B) are based on the uncertainty of the linear regressions in the G' *vs.* temperature graphs. C) G' *vs.* temperature for reaction (3); solid circles show reversal experiments where natron growth occurred and open circles indicate where trona growth occurred. Note a best fit linear regression (dashed line) does not fit between all the bracketed data points for reaction (3). Predicted *G' vs* temperature (solid line), calculated from data derived for natron and trona [reactions (1) and (2)], fits between the bracketed data points.

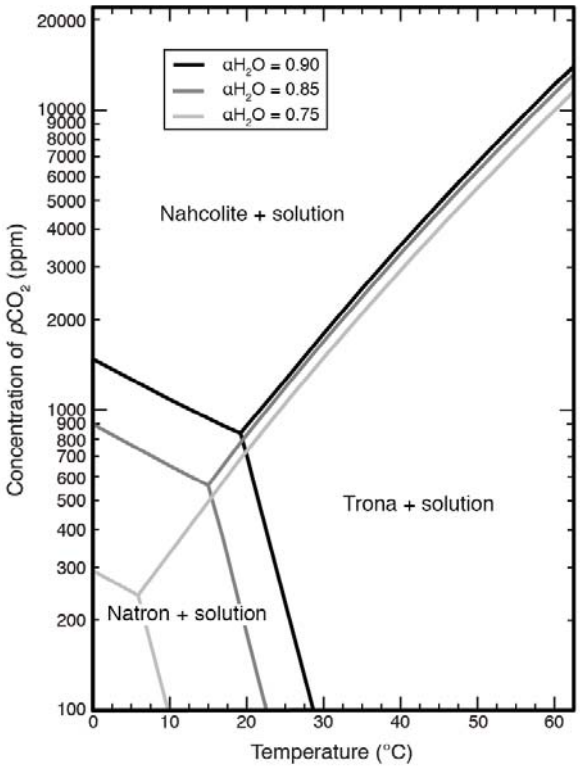

Figure DR5. Phase diagram showing changes in the stability fields of sodium carbonate minerals as a function of the activity of H_2O in pCO_2-temperature space. Solid black line represents all minerals in the Na_2CO_3-$NaHCO_3$-H_2O-CO_2 system at an activity of H_2O of 0.90. Dark gray and light gray lines model how the invariant point array shifts to lower pCO_2 concentrations and temperatures by decreasing the activity of H_2O (0.85 and 0.75 respectively). The light gray line shows a downward shift of the invariant point when the system is at halite (NaCl) saturation, and demonstrates that nahcolite can form at low temperatures and low pCO_2 when the activity of H_2O is low. This may explain the formation of nahcolite in Owens Lake, California in 1970-1971 during the winter months and at night when temperatures were low (Smith et al., 1987).

Table DR1. Experimental conditions and results for reaction (1), 3nahcolite + H_2O = trona + CO_2.

Code	T (°C)	pCO_2 (ppm)[†]	time (h)	Comments	Fluid content (wt %)	Average Peak-Area ratio (Nahc/Tr)[§]
Nahc-Tr-m1 starting mixture	23[*]	400-500[*]	N/A	nahcolite + trona	N/A	0.644 (0.005)
Nahc-Tr-m1-4-1,2,3	15	1270	24	nahcolite growth; breakdown of trona	2.5-3.1	0.761 (0.002)
Nahc-Tr-m1-5-1,2,3	20	1270	19	nahcolite growth; breakdown of trona	3.1-3.3	0.711 (0.01)
Nahc-Tr-m1-6-2,3,4	25	1270	22	nahcolite growth; breakdown of trona	2.9-3.1	0.687 (0.004)
Nahc-Tr-m1-7-1,2,3	30	1270	20	trona growth; breakdown of nahcolite	2.8-3.1	0.624 (0.007)
Nahc-Tr-m1-8-1,2,3	35	1270	24	trona growth; breakdown of nahcolite	2.7-3.1	0.588 (0.005)
Nahc-Tr-m1-9-1,2,3	40	1270	23	trona growth; breakdown of nahcolite	2.8-3.0	0.576 (0.004)
Nahc-Tr-m2 starting mixture	23[*]	400-500[*]	N/A	nahcolite + trona	N/A	0.771 (0.02)
Nahc-Tr-m2-2-1,2,3	15	1469	24	nahcolite growth; breakdown of trona	2.1-2.5	0.854 (0.006)
Nahc-Tr-m2-3-1,2,3	20	1469	23	nahcolite growth; breakdown of trona	2.7-3.0	0.838 (0.01)
Nahc-Tr-m2-4-1,2,3	25	1469	23	nahcolite growth; breakdown of trona	2.8-3.1	0.792 (0.03)
Nahc-Tr-m2-5-1,2,3	30	1469	24	trona growth; breakdown of nahcolite	2.5-2.9	0.741 (0.01)
Nahc-Tr-m2-6-1,2,3	35	1469	23	trona growth; breakdown of nahcolite	2.1-2.5	0.694 (0.02)
Nahc-Tr-m2-7-1,2,3	40	1469	21	trona growth; breakdown of nahcolite	2.3-3.0	0.632 (0.04)
Nahc-Tr-m3 starting mixture	23[*]	400-500[*]	N/A	nahcolite + trona	N/A	0.695 (0.05)
Nahc-Tr-m3-2-1,2,3	20	2047	24	nahcolite growth; breakdown of trona	2.8	0.867 (0.01)
Nahc-Tr-m3-3-1,2,3	25	2047	23	nahcolite growth; breakdown of trona	2.8-3.0	0.796 (0.03)
Nahc-Tr-m3-4-1,2,3	30	2047	25	nahcolite growth; breakdown of trona	2.7-3.1	0.736 (0.008)
Nahc-Tr-m3-5-3,4,5	35	2047	20	trona growth; breakdown of nahcolite	2.8-3.0	0.668 (0.01)
Nahc-Tr-m3-6-3,4,5	40	2047	19	trona growth; breakdown of nahcolite	2.6-3.0	0.619 (0.004)
Nahc-Tr-m3-7-1,2,3	50	2047	22	trona growth; breakdown of nahcolite	2.6-2.9	0.587 (0.005)

Nahc-Tr-m4 starting mixture	23*	400-500*	N/A	nahcolite + trona	N/A	0.670 (0.02)
Nahc-Tr-m4-3-1,2,3	25	2935	24	nahcolite growth; breakdown of trona	2.9-3.1	0.854 (0.04)
Nahc-Tr-m4-4-1,0,1	30	2935	19	nahcolite growth; breakdown of trona	2.5-2.8	0.771 (0.02)
Nahc-Tr-m4-5-1,2,3	35	2935	25	nahcolite growth; breakdown of trona	2.8-2.9	0.717 (0.01)
Nahc-Tr-m4-6-1,2,3	40	2935	20	trona growth; breakdown of nahcolite	2.6-2.7	0.635 (0.03)
Nahc-Tr-m4-7-1,2,3	55	2935	26	trona growth; breakdown of nahcolite	2.6-3.0	0.606 (0.01)
Nahc-Tr-m4-8-1,2,3	60	2935	23	trona growth; breakdown of nahcolite	2.7-2.8	0.576 (0.007)
Nahc-Tr-m5 starting mixture	23*	400-500*	N/A	nahcolite + trona	N/A	0.654 (0.02)
Nahc-Tr-m5-10-1,2,3	25	4999	18	nahcolite growth; breakdown of trona	2.8-2.9	0.794 (0.008)
Nahc-Tr-m5-11-1,2,3	35	4999	23	nahcolite growth; breakdown of trona	2.7-2.9	0.725 (0.03)
Nahc-Tr-m5-12-1,2,3	40	4999	24	nahcolite growth; breakdown of trona	2.7-3.0	0.688 (0.01)
Nahc-Tr-m5-13-1,2,3	48	4999	21	trona growth; breakdown of nahcolite	2.6-2.8	0.619 (0.02)
Nahc-Tr-m5-14-1,2,3	55	4999	30	trona growth; breakdown of nahcolite	2.7-2.8	0.593 (0.005)
Nahc-Tr-m5-16-1,2,3	60	4999	28	trona growth; breakdown of nahcolite	2.7-2.9	0.528 (0.02)
Nahc-Tr-m6 starting mixture	23*	400-500*	N/A	nahcolite + trona	N/A	1.155 (0.11)
Nahc-Tr-m6-13-1,2,3	25	7854	35	nahcolite growth; breakdown of trona	2.8-3.0	1.352 (0.03)
Nahc-Tr-m6-14-1,2,3	35	7854	21	nahcolite growth; breakdown of trona	2.8-2.9	1.284 (0.04)
Nahc-Tr-m6-11-1,2,3	45	7854	19	nahcolite growth; breakdown of trona	2.7-3.0	1.213 (0.03)
Nahc-Tr-m6-10-1,2,3	53	7854	26	trona growth; breakdown of nahcolite	2.8-2.9	1.118 (0.02)
Nahc-Tr-m6-8-1,2,3	60	7854	17	trona growth; breakdown of nahcolite	2.7-2.8	0.915 (0.02)
Nahc-Tr-m6-5-1,2,3	65	7854	24	trona growth; breakdown of nahcolite	2.6-2.8	0.896 (0.02)
Nahc-Tr-m7 starting mixture	23*	400-500*	N/A	nahcolite + trona	N/A	0.624 (0.02)
Nahc-Tr-m7-15-1,2,3	25	9915	23	nahcolite growth; breakdown of trona	2.9-3.0	0.820 (0.04)
Nahc-Tr-m7-18-1,2,3	30	9915	20	nahcolite growth; breakdown of trona	2.8-2.9	0.813 (0.02)
Nahc-Tr-m7-19-1,2,3	35	9915	21	nahcolite growth; breakdown of trona	2.9-3.1	0.752 (0.05)
Nahc-Tr-m7-21-1,2,3	45	9915	23	nahcolite growth; breakdown of trona	2.7-2.9	0.708 (0.02)

Nahc-Tr-m7-23-1,2,3	55	9915	25	nahcolite growth; breakdown of trona	2.7-2.8	0.667 (0.02)
Nahc-Tr-m7-24-1,2,3	60	9915	27	trona growth; breakdown of nahcolite	2.8-2.9	0.539 (0.07)
Nahc-Tr-m7-25-1,2,3	60	9915	21	trona growth; breakdown of nahcolite	2.8-3.1	0.500 (0.03)
Nahc-Tr-m7-27-1,2,3	75	9915	24	trona growth; breakdown of nahcolite	2.8-3.0	0.387 (0.08)

[*]Measured temperature and pCO_2 concentrations in the laboratory; ambient laboratory pCO_2 concentrations varied from ~ 400 to 500 ppm.

[†]Concentration of CO_2 gas standards had uncertainties of ± 2% ppm.

[§]Ratio Average and standard deviation (in parentheses) of the ratio of the nahcolite peak area/trona peak area for three replicate experiments.

Table DR2. Experimental conditions and results for reaction (2), 2nahcolite + $9H_2O$ = natron + CO_2.

Code	T (°C)	pCO_2 (ppm)[†]	time (h)	Comments	Fluid content (wt %)	Average Peak-Area ratio (Nahc/Nat)[#]
Nahc-nat-m1 starting mixture	20[*]	400-500[*]	0.25[§]	nahcolite + natron + solution	26.3	1.322
Nahc-nat-m1-1	10	803	1	natron growth; breakdown of nahcolite	26.3	0.256
Nahc-nat-m1-2	10	1001	0.75	natron growth; breakdown of nahcolite	26.3	0.562
Nahc-nat-m1-3	10	1270	0.75	nahcolite growth; breakdown of natron	26.3	1.534
Nahc-nat-m2 starting mixture	20[*]	400-500[*]	0.25[§]	nahcolite + natron + solution	26.3	1.005
Nahc-nat-m2-1	10	803	1	natron growth; breakdown of nahcolite	26.3	0.533
Nahc-nat-m2-2	10	1001	1	natron growth; breakdown of nahcolite	26.3	0.846
Nahc-nat-m2-3	10	1469	1	nahcolite growth; breakdown of nahcolite	26.3	1.202
Nahc-nat-m3 starting mixture	21[*]	400-500[*]	0.25[§]	nahcolite + natron + solution	26.3	0.683
Nahc-nat-m3-1	18	1469	1	nahcolite growth; breakdown of natron	26.3	1.322
Nahc-nat-m3-2	18	499	1	natron growth; breakdown of nahcolite	26.3	0.412
Nahc-nat-m3-3	10	499	1	natron growth; breakdown of nahcolite	26.3	0.209
Nahc-nat-m3-4	18	1270	1	nahcolite growth; breakdown of natron	26.3	1.139
Nahc-nat-m4 starting mixture	20[*]	400-500[*]	0.25[§]	natron + natron + solution	26.3	1.283
Nahc-nat-m4-5	15	1001	1	nahcolite growth; breakdown of natron	26.3	1.421
Nahc-nat-m4-6	17	803	1	natron growth; breakdown of nahcolite	26.3	1.074
Nahc-nat-m4-7	19	1001	1	nahcolite growth; breakdown of natron	26.3	1.673
Nahc-nat-m4-8	21.5	803	1	natron + trona growth; breakdown of nahcolite	26.3	0.847

[*]Measured temperature and pCO_2 concentrations in the laboratory; ambient laboratory pCO_2 concentrations varied from ~ 400 to 500 ppm.

[†]Concentration of CO_2 gas standards had uncertainties of ± 2% ppm.

[§]X-ray diffraction scan time. Sample was scanned in a sealed heating stage chamber at room atmospheric CO_2 concentrations and water-vapor saturated conditions.

[#]Ratio of nahcolite peak area/natron peak area.

Table DR3. Experimental conditions and results for reaction (3), 2trona + 25H_2O = 3natron + CO_2.

Code	T (°C)	pCO_2 (ppm)[†]	time (h)	Comments	Fluid content (wt %)	Average Peak-Area ratio (Tr/Nat)[#]
Tr-nat-m1 starting mixture	21[*]	400-500[*]	0.25[§]	trona + natron + solution	25	1.467
Tr-nat-m1-1	10	803	22	natron growth; trace amount of trona	25	0.063
Tr-nat-m1-2	15	803	27	natron growth; trace amount of trona	25	0.072
Tr-nat-m1-3	17	803	25	natron growth; trace amount of trona	25	0.073
Tr-nat-m1-4	20	803	26	trona growth; trace amount of natron	25	2.562
Tr-nat-m1-5	25	803	25	trona growth; complete breakdown of natron	25	5.087
Tr-nat-m3 starting mixture	22[*]	400-500[*]	0.25[§]	trona + natron + solution	25	0.958
Tr-nat-m3-1	15	803	26	natron growth; trace amount of trona	25	0.015
Tr-nat-m3-2	17	803	23	natron growth; trace amount of trona	25	0.429
Tr-nat-m3-3	19	803	25	natron growth decreases; trona growth increases	25	1.645
Tr-nat-m3-4	25	803	24	trona growth; complete breakdown of natron	25	6.631
Tr-nat-m4 starting mixture	22[*]	400-500[*]	0.25[§]	trona + natron + solution	25	0.865
Tr-nat-m4-1	10	630	25	natron growth; trace amount of trona	25	0.006
Tr-nat-m4-2	15	630	24	natron growth; trace amount of trona	25	0.013
Tr-nat-m4-3	18	630	26	natron growth; trace amount of trona	25	0.249
Tr-nat-m4-4	21	630	24	trona growth; trace amount of natron	25	3.457
Tr-nat-m4-5	24	630	25	trona growth; complete breakdown of natron	25	6.732
Tr-nat-m5 starting mixture	22[*]	400-500[*]	0.25[§]	trona + natron + solution	25	0.786
Tr-nat-m5-1	17	545	24	natron growth; trace amount of trona	25	0.032
Tr-nat-m5-2	19	545	25	natron growth; trace amount of trona	25	0.476
Tr-nat-m5-3	22	545	23	trona growth; trace amount of natron	25	2.461
Tr-nat-m5-4	25	545	21	trona growth; complete breakdown of natron	25	7.973
Tr-nat-m7 starting mixture	22[*]	400-500[*]	0.25[§]	trona + natron + solution	25	1.361
Tr-nat-m7-1	10	545	25	natron growth; trace amount of trona	25	0.008
Tr-nat-m7-2	19	545	23	natron growth decreases; trona growth increases	25	0.589
Tr-nat-m7-3	22	545	24	metastability of natron; trona growth	25	2.163
Tr-nat-m7-4	22	545	22	trona growth; complete breakdown of natron	25	5.463

[*]Measured temperature and pCO_2 concentrations in the laboratory; ambient laboratory pCO_2 concentrations varied from ~ 400 to 500 ppm.

[†]Concentration of CO_2 gas standards had uncertainties of ± 2% ppm.

[§]X-ray diffraction scan time. Sample was scanned in a sealed heating stage chamber at room atmospheric CO_2 concentrations and water-vapor saturated conditions.

[#]Ratio of trona peak area/natron peak area.

Table DR4. $\Delta H^{\circ}_{f,298}$ and S°_{298} values for trona and natron derived in this study compared to previously reported values

Compound/Reference	$\Delta H^{\circ}_{f,298}$ (kJ/mol)	S°_{298} (kJ/K•mol)
Na_2CO_3•$NaHCO_3$•$2H_2O_{(trona)}$		
This study	-2658.40 ± 0.55*	0.2868 ± 0.0029*
Vanderzee (1982)	-2682.11 ± 0.44	0.30313 ± 0.0170
Na_2CO_3•$10H_2O_{(natron)}$		
This study	-4094.49 ± 0.60*	0.49943 ± 0.002*
Vanderzee (1982)	-4079.78 ± 0.90	0.56274 ± 0.0115

*Uncertainties are constrained by experimental data.

Supplementary Information References (Not in Manuscript)

Badger, M.P.S., Lear, C.H., Pancost, R.D., Foster, G.L., Bailey, T.R., Leng, M.J., and Abels, H.A., 2013a, CO_2 drawdown following the middle Miocene expansion of the Antarctic Ice Sheet: Paleoceanography, v. 28, p. 42-53.

Badger, M. P. S., Schmidt, D. N., Mackensen, A., and Pancost, R. D., 2013b, High-resolution alkenone palaeobarometry indicates relatively stable pCO_2 during the Pliocene (3.3–2.8 Ma): Philosophical Transactions of the Royal Society of America, v. 371, p. 2013094.

Bartoli, G., Hönisch, B., and Zeebe, R.E., 2011, Atmospheric CO_2 decline during the Pliocene intensification of Northern Hemisphere glaciations: Paleoceanography, v. 26, p. PA4213.

Beerling, D.J., Lomax, B.H., Royer, D.L., Upchurch, G.R., and Kump, L.R., 2002, An atmospheric pCO_2 reconstruction across the Cretaceous-Tertiary boundary from leaf megafossils: Proceedings of the National Academy of Sciences U.S.A., v. 99, p. 7836-7840.

Doria, G., Royer D.L., Wolfe, A.P., Fox, A., Westgate, J.A., and Beerling, D.J., 2011, Declining atmospheric CO_2 during the late Middle Eocene climate transition: American Journal of Science, v. 311, p. 63-75.

Erdei, B., Utescher, T., Hably, L., Tamás, J., Roth-Nebelsick, A., and Grein, M., 2012, Early Oligocene continental climate of the Palaeogene Basin (Hungary and Slovenia) and the surrounding area: Turkish Journal of Earth Science, v. 21, p. 153-186.

Foster, G.L., Lear, C.H., and Rae, J.W.B., 2012, The evolution of pCO_2, ice volume and climate during the middle Miocene: Earth Planetary Science Letters, v. 341-344, p. 243-254.

Gradstein, F.M., Ogg, J.G., and Smith, A.G., eds., 2004, A Geologic Time Scale 2004: Cambridge, Cambridge University Press.

Grein, M., Konrad, W., Wilde, V., Utescher, T., and Roth-Nebelsick, A., 2011, Reconstruction of atmospheric CO_2 during the early Middle Eocene by application of a gas exchange model to fossil plants from the Messel Formation, Germany: Palaeogeography Palaeoclimatology Palaeoecology, v. 309, p. 383-391.

Grein, M., Oehm, C., Konrad, W., Utescher, T., Kunzmann, L., and Roth-Nebelsick, A., 2013, Atmospheric CO_2 from the late Oligocene to early Miocene based on photosynthesis data and fossil leaf characteristics: Palaeogeography Palaeoclimatology Palaeoecology, v. 374, p. 41-51.

Hatch, J.R., 1972, Phase relationships in part of the system sodium carbonate calcium carbonate-carbon dioxide-water at one atmosphere pressure [Ph.D. thesis]: Urbana, University of Illinois, 85 p.

Helvaci, C., 1998, The Beypazari trona deposits, Ankara Province, Turkey. *in* Dyni, J. R. and Jones, R.W. eds., Proceedings of the First International Soda Ash Conference: Laramie, Wyoming State Geological Survey, Public Information Circular 40, p. 67-103.

Huang, C., Retallack, G.J., Wang, C. & Huang, Q., 2013, Paleoatmospheric pCO_2 fluctuations across the Cretaceous-Tertiary boundary recorded from paleosol carbonates in NE China: Palaeogeography Palaeoclimatology Palaeoecology, v. 385, p. 95-105.

Koch, P.L., Zachos, J.C., and Gingerich, P.D., 1992, Correlation between isotope records in marine and continental carbon reservoirs near the Palaeocene/Eocene boundary: Nature, v. 358, p. 319-322.

Kürshner, W.M., 1996, Leaf stomata as biosensors of paleoatmospheric CO_2 Levels: Laboratory of Palaeobotany and Palynology Contributions Series, v. 5, p. 1-153.

Kürschner, W.M., Kvacek, Z., and Dilcher, D.L., 2008, The impact of Miocene atmospheric carbon dioxide fluctuations on climate and the evolution of terrestrial ecosystems: Proceedings of the National Academy of Sciences U.S.A., v. 105, p. 449-453.

Nordt, L., Atchley, S., and Dworkin, S.I., 2002, Paleosol barometer indicates extreme fluctuations in atmospheric CO_2 across the Cretaceous-Tertiary boundary: Geology, v. 30, p. 703-706.

Pearson, P.N., Foster, G.L., and Wade, B.S., 2009, Atmospheric carbon dioxide through the Eocene-Oligocene climate transition: Nature, v. 461, p. 1110-1113.

Quade, J., Solounias, N., and Cerling, T.E., 1994, Stable isotopic evidence from paleosol carbonates and fossil teeth in Greece for forest or woodlands over the past 11 Ma: Palaeogeography Palaeoclimatology Palaeoecology, v. 108, p. 41-53.

Quade, J., and Cerling, T.E., 1995, Expansion of C_4 grasses in the Late Miocene of Northern Pakistan: evidence from stable isotopes in paleosols: Palaeogeography Palaeoclimatology Palaeoecology, v. 115, p. 91-116.

Retallack, G.J., 2009a, Greenhouse crises of the past 300 million years: Geological Society of America Bulletin, v. 121, p. 1441-1455.

Retallack, G.J., 2009b, Refining a pedogenic-carbonate CO_2 paleobarometer to

quantify a middle Miocene greenhouse spike: Palaeogeography Palaeoclimatology Palaeoecology, v. 281, p. 57-65.

Robie, R.A., and Hemingway, B.S., 1995, Thermodynamic properties of minerals and related substances at 298.15 K and1 Bar (10^5 Pascals) pressure and at higher temperatures: USGS Bulletin, v. 2131, p. 461.

Roth-Nebelsick, A., Grein, M., Utescher, T., and Konrad, W., 2012, Stomatal pore length change in leaves of *Eotrigonobalanus furcinervis* (Fagaceae) from the Late Eocene to the Latest Oligocene and its impact on gas exchange and CO_2 reconstruction: Review of Palaeobotany and Palynology, v. 174, p. 106-112.

Seki, O., Foster, G.L., Schmidt, D.N., Mackensen, A., Kawamura, K., and Pancost, R.D., 2010, Alkenone and boron-based Pliocene pCO_2 records: Earth and Planetary Science Letters, v. 292, p.201-211.

Smith, G. I., 1979, Subsurface stratigraphy and geochemistry of Late Quaternary evaporites, Searles Lake, California. USGS Professional Paper, v. 1043, p. 1-130.

Stults, D.Z., Wagner-Cremer, F., and Axsmith, B.J., 2011, Atmospheric paleo-CO_2 estimates based on *Taxodium distichum* (Cupressaceae) fossils from the Miocene and Pliocene of eastern North America: Palaeogeography Palaeoclimatology Palaeoecology, v. 309, p. 327-332.

Van der Burgh, J., Visscher, H., Dilcher, D.L., and Kürschner, W.M., 1993, Paleoatmospheric signatures in Neogene fossil leaves. Science, v. 260, p. 1788-1790.

Vanderzee, C.E., 1982, Thermodynamic relations and equilibria in (Na_2CO_3 + $NaHCO_3$ + H_2O): standard Gibbs energies of formation and other properties of sodium hydrogen carbonate, sodium carbonate heptahydrate, sodium carbonate decahydrate, trona: (Na_2CO_3•$NaHCO_3$•$2H_2O$), and Wegscheider's salt (Na_2CO_3•$3NaHCO_3$): Journal of Chemical Thermodynamics, v. 14, p. 219-238.